

Attracting and repelling Lagrangian coherent structures from a single computation

Mohammad Farazmand^{1,2} and George Haller²

¹*Department of Mathematics, ETH Zürich, 8092 Zürich, Switzerland*

²*Institute for Mechanical Systems, ETH Zürich, 8092 Zürich, Switzerland*

(Received 18 January 2013; accepted 19 March 2013; published online 12 April 2013)

Hyperbolic Lagrangian Coherent Structures (LCSs) are locally most repelling or most attracting material surfaces in a finite-time dynamical system. To identify both types of hyperbolic LCSs at the same time instance, the standard practice has been to compute repelling LCSs from future data and attracting LCSs from past data. This approach tacitly assumes that coherent structures in the flow are fundamentally recurrent, and hence gives inconsistent results for temporally aperiodic systems. Here, we resolve this inconsistency by showing how both repelling and attracting LCSs are computable at the same time instance from a single forward or a single backward run. These LCSs are obtained as surfaces normal to the weakest and strongest eigenvectors of the Cauchy-Green strain tensor. © 2013 AIP Publishing LLC. [<http://dx.doi.org/10.1063/1.4800210>]

Repelling and attracting Lagrangian coherent structures (LCSs) are material surfaces that govern mixing patterns in complex dynamical systems. Recent developments made the accurate computation of both types of structures possible, but not for the same data set: repelling LCSs are invariably obtained from future data, and attracting LCSs from past data. For temporally aperiodic flows, this practice locates repelling and attracting LCSs for two different finite-time dynamical systems. Here, we resolve this inconsistency by showing that both types of LCSs can be computed at the same time instance from the same data set.

2012; Haller and Beron-Vera, 2012) are now available for their extraction from flow data.

All available hyperbolic LCS methods fundamentally seek locations of large particle separation. They will highlight repelling LCS positions at some initial time $t = a$ from a forward-time analysis of the flow over a finite time-interval $[a, b]$. Similarly, these methods reveal attracting LCSs at the final time $t = b$ from a backward-time analysis of the flow over $[a, b]$. The complete hyperbolic LCS distribution at a fixed time $t \in [a, b]$ is, therefore, not directly available.

Two main approaches have been employed to resolve this issue (see Figure 1 for an illustration):

I. INTRODUCTION

The differential equations governing a number of physical processes are only known as observational or numerical data sets. Examples include oceanic and atmospheric particle motion, whose velocity field is only known at discrete locations, evolving aperiodically over a finite time-interval of availability. For such temporally aperiodic data sets, classic dynamical concepts—such as fixed points, periodic orbits, stable and unstable manifolds, or chaotic attractors—are either undefined or nongeneric.

Instead of relying on classic concepts, one may seek influential surfaces responsible for the formation of observed trajectory patterns over a finite time frame of interest. Such a surface is necessarily a material surface, i.e., a codimension-one set of initial conditions evolving with the flow. Among material surfaces, an attracting LCS is defined as a locally most attracting material surface in the phase space (Haller and Yuan, 2000; Haller, 2011). Repelling LCSs are defined as locally most repelling material surfaces, i.e., attracting LCSs in backward-time. Repelling and attracting LCSs together are referred to as hyperbolic LCSs. Both heuristic detection methods (Peacock and Dabiri, 2010) and rigorous variational algorithms (Haller, 2011; Farazmand and Haller,

1. Approach I: Divide the finite time interval of interest as $[a, b] = [a, t_0] \cup [t_0, b]$. Compute repelling LCSs from a forward run over $[t_0, b]$, and attracting LCSs from the backward run over $[a, t_0]$ (see, e.g., Lekien and Ross (2010); Lipinski and Mohseni (2010)). Both repelling and attracting LCSs are then obtained at the same time slice t_0 . However, they correspond to two different finite-time dynamical systems: one defined over $[a, t_0]$ and the other over $[t_0, b]$. This approach works well for a roughly T -periodic system, when $t_0 - a$ and $b - t_0$ are integer multiples of T . In general, however, hyperbolic LCSs computed over $[a, t_0]$ and over $[t_0, b]$ do not evolve into each other as t_0 is varied, and hence the resulting structures are not dynamically consistent. In addition, one cannot identify attracting LCSs at time a or repelling LCSs at time b from this approach.

2. Approach II: Extract repelling LCSs at the initial time a from a forward run over $[a, b]$; extract attracting LCSs at the final time b from a backward run over $[a, b]$. Obtain repelling LCSs at any time $t_0 \in [a, b]$ by advecting repelling LCSs from a to t_0 under the flow. Similarly, obtain attracting LCSs at any time $t_0 \in [a, b]$ by advecting attracting LCSs from b to t_0 under the flow. This approach identifies LCSs based on the full available data, and provides dynamically consistent surfaces that evolve into

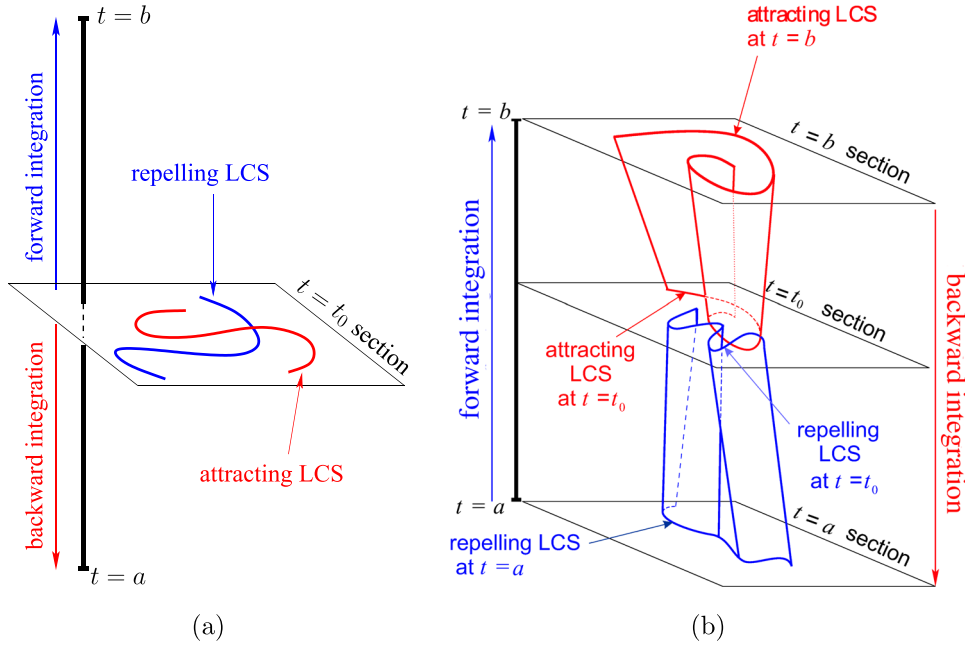


FIG. 1. Schematic illustration of approach I (a) and approach II (b) in the extended phase space.

each other as t_0 varies (Haller, 2011; Farazmand and Haller, 2012). Since the forward-time advection of a repelling LCS (as well as the backward-time advection of an attracting LCS) is numerically unstable (see Figure 2), this approach requires extra care to suppress growing instabilities (Farazmand and Haller, 2012). Even under well-controlled instabilities, however, a further issue arises in near-incompressible flows: repelling LCSs shrink exponentially under forward-advection, and attracting LCSs shrink exponentially under backward-advection. Therefore, while the LCSs obtained in this fashion are dynamically consistent, they require substantial numerical effort to extract and may still reveal little about the dynamics.

Here, we develop a new approach that keeps the dynamical consistency of approach II but eliminates the instability and shrinkage of advected LCSs. Our key observation is that attracting LCSs can also be recovered as codimension-one hypersurfaces normal to the weakest eigenvector field of the forward Cauchy-Green strain tensor. These *stretch-surfaces* are obtained from the same forward-time calculation that reveals repelling LCSs as *strain-surfaces*, i.e., codimension-one surfaces normal to the dominant eigenvector of the forward Cauchy-Green strain tensor (Farazmand and Haller, 2012). The locally most compressing strain-surfaces and the locally most expanding stretch-surfaces then reveal repelling and attracting LCSs at the same initial time a based on a single forward-time calculation over $[a, b]$.

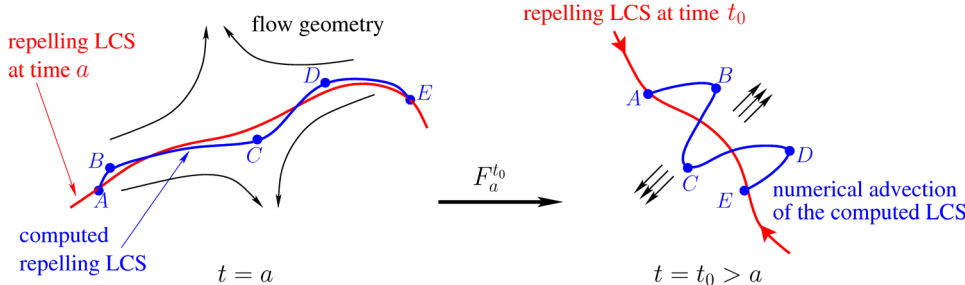


FIG. 2. The errors in the computation of a repelling LCS grow exponentially as the LCS is advected forwards in time. The same statement holds for the backward-time advection of an attracting LCS.

We demonstrate the results on three examples: an autonomous Duffing oscillator (Sec. VA), a direct numerical simulation of two-dimensional turbulence (Sec. VB), and the three-dimensional classic ABC flow (Sec. VC).

II. PRELIMINARIES AND NOTATION

Consider the dynamical system

$$\dot{x} = u(x, t), \quad x \in U \subset \mathbb{R}^n, \quad t \in I = [a, b], \quad (1)$$

where $u : U \times I \rightarrow \mathbb{R}^n$ is a sufficiently smooth velocity field. For $t_0, t \in I$, define the flow map

$$F_{t_0}^t : U \rightarrow U \\ x_0 \mapsto x(t; t_0, x_0), \quad (2)$$

as the unique one-to-one map that takes the initial condition x_0 to its time- t position $x(t; t_0, x_0)$ under system (1).

The *forward Cauchy-Green strain tensor* over the time interval I is defined in terms of the flow gradient ∇F_a^b as

$$C^f = (\nabla F_a^b)^T \nabla F_a^b. \quad (3)$$

At each initial condition $x_0 \in U$, the tensor $C^f(x_0)$ is represented by a symmetric, positive definite, $n \times n$ matrix with an orthonormal set of eigenvectors $\{\xi_k^f(x_0)\}_{1 \leq k \leq n}$, and with a corresponding set of eigenvalues $\{\lambda_k^f(x_0)\}_{1 \leq k \leq n}$ satisfying

$$C^f(x_0)\xi_k^f(x_0) = \lambda_k^f(x_0)\xi_k^f(x_0), \quad k \in \{1, 2, \dots, n\}, \quad (4a)$$

$$0 < \lambda_1^f(x_0) \leq \lambda_2^f(x_0) \leq \dots \leq \lambda_n^f(x_0). \quad (4b)$$

These invariants of the Cauchy–Green strain tensor characterize the deformation experienced by trajectories starting close to x_0 . If a unit sphere is placed at x_0 , its image under the linearized flow map ∇F_a^b will be an ellipsoid whose principal axes align with the eigenvectors $\{\xi_k^f(x_0)\}_{1 \leq k \leq n}$ and have corresponding lengths $\{\lambda_k^f(x_0)\}_{1 \leq k \leq n}$.

Similarly, the *backward Cauchy–Green strain tensor* over the time interval I is defined as

$$C^b = (\nabla F_b^a)^\top \nabla F_b^a. \quad (5)$$

Its eigenvalues $\{\lambda_k^b(x_0)\}_{1 \leq k \leq n}$ and orthonormal eigenvectors $\{\xi_k^b(x_0)\}_{1 \leq k \leq n}$ satisfy similar properties as those in Eq. (4). Their geometric meaning is similar to that of the invariants of C^f , but in backward time.

III. REPELLING AND ATTRACTING LCSs

A repelling LCS over the time interval I is a codimension-one material surface that is pointwise more repelling over I than any nearby material surface. If $\mathcal{R}(t)$ represents the time- t position of such a LCS, then the initial LCS position $\mathcal{R}(a)$ must be everywhere orthogonal to the most-stretching eigenvector ξ_n^f of the forward Cauchy–Green strain tensor C^f (Haller, 2011; Haller and Beron-Vera, 2012). Specifically, we must have

$$T_{x_a}\mathcal{R}(a) \perp \xi_n^f(x_a), \quad (6)$$

for any point $x_a \in \mathcal{R}(a)$, where $T_{x_a}\mathcal{R}(a)$ denotes the tangent space of $\mathcal{R}(a)$ at point x_a .

Similarly, an attracting LCS over the time interval I is a codimension-one material surface that is pointwise more attracting over I than any nearby material surface. If $\mathcal{A}(t)$ is the time- t position of an *attracting* LCS, its final position $\mathcal{A}(b)$ satisfies

$$T_{x_b}\mathcal{A}(b) \perp \xi_n^b(x_b), \quad (7)$$

for all points $x_b \in \mathcal{A}(b)$. That is, the time- b position of attracting LCS is everywhere orthogonal to the eigenvector ξ_n^b of the backward Cauchy–Green strain tensor C^b .

The relation (6) enables the construction of repelling LCS candidates at time $t = a$, while Eq. (7) enables the construction of attracting LCS candidates at the final time $t = b$ (see, e.g., Farazmand and Haller (2012); Hadjighasem, Farazmand, and Haller (2012)). Since LCSs are constructed as material surfaces, they move with the flow. Therefore, LCS positions at an intermediate time $t_0 \in [a, b]$ are, in principle, uniquely determined by their end-positions

$$\mathcal{R}(t_0) = F_a^{t_0}(\mathcal{R}(a)), \quad \mathcal{A}(t_0) = F_b^{t_0}(\mathcal{A}(b)). \quad (8)$$

As discussed in the introduction, however, using the advection formulae (8) leads to numerical instabilities. This is because the material surfaces involved are unstable in the

time direction they are advected in. This instability can only be controlled by employing a high-end numerical integrator which refines the advected surface when large stretching develops. Even under high-precision advection, however, the end-result is an exponentially shrinking surface which only captures subsets of the most influential material surfaces.

IV. MAIN RESULT

Here, we present a direct method to identify both attracting and repelling LCSs at the same time instance, using the same finite time-interval. These surfaces, therefore, are based on the assessment of the same finite-time dynamical system, avoiding the dynamical inconsistency we reviewed for approach I in the Introduction.

In particular, we show that the initial position of an attracting LCS, $\mathcal{A}(a)$, is everywhere orthogonal to the weakest eigenvector ξ_1^f of the tensor C^f . This, together with the orthogonality of the initial repelling LCS position $\mathcal{R}(a)$ to the dominant eigenvector ξ_n^f of C^f , allows for the simultaneous construction of attracting and repelling LCSs at time $t = a$, utilizing the same time interval $[a, b]$. All this renders the computation of the backward Cauchy–Green strain tensor C^b unnecessary.

Similarly, if locating the hyperbolic structures based on past flow data (now-casting) is of interest, current positions of repelling and attracting LCSs can be located from a single backward-time integration starting from the present time. In this case, the current position of an attracting LCS is everywhere orthogonal to the dominant eigenvector ξ_n^b of the backward Cauchy–Green strain tensor C^b . Likewise, the current positions of repelling LCSs are everywhere orthogonal to the weakest eigenvector ξ_1^b of the tensor C^b .

We start with definitions of the surfaces involved in our results:

Definition 1 (Strain-surface). Let $\mathcal{M}(t)$ be an $(n - 1)$ -dimensional smooth material surface in U , evolving under the flow map over the time interval $I = [a, b]$ as $\mathcal{M}(t) = F_a^t(\mathcal{M}(a))$. Denote the tangent space of \mathcal{M} at a point $x \in \mathcal{M}$ by $T_x\mathcal{M}$.

- (i) $\mathcal{M}(t)$ is called a *forward strain-surface* if $\mathcal{M}(a)$ is everywhere normal to the eigenvector field ξ_n^f , i.e.,

$$T_{x_a}\mathcal{M}(a) \perp \xi_n^f(x_a), \quad \forall x_a \in \mathcal{M}(a).$$

- (ii) $\mathcal{M}(t)$ is called a *backward strain-surface* if $\mathcal{M}(b)$ is everywhere normal to the eigenvector field ξ_n^b , i.e.,

$$T_{x_b}\mathcal{M}(b) \perp \xi_n^b(x_b), \quad \forall x_b \in \mathcal{M}(b).$$

Strain-surfaces are generalizations of the strainlines introduced in Farazmand and Haller (2012) and Haller and Beron-Vera (2012) in the theory of hyperbolic LCSs for two-dimensional flows. By contrast, the stretch-surfaces appearing in the following definition have not yet been used even in two-dimensional LCS detection.

Definition 2 (Stretch-surface). Let $\mathcal{M}(t)$ be an $(n - 1)$ -dimensional material surface as in Definition 1.

- (i) $\mathcal{M}(t)$ is called a *forward stretch-surface* if $\mathcal{M}(a)$ is everywhere normal to the eigenvector field ξ_1^f , i.e.,

$$T_{x_a}\mathcal{M}(a) \perp \xi_1^f(x_a), \quad \forall x_a \in \mathcal{M}(a).$$

- (ii) $\mathcal{M}(t)$ is called a *backward stretch-surface* if $\mathcal{M}(b)$ is everywhere normal to the eigenvector field ξ_1^b , i.e.,

$$T_{x_b}\mathcal{M}(b) \perp \xi_1^b(x_b), \quad \forall x_b \in \mathcal{M}(b).$$

By definition, the local orientation of a forward strain-surface is known at the initial time $t=a$. The following theorem determines the local orientation of the same strain-surface at the final time $t=b$, rendering the forward-advection of the surface unnecessary. The same theorem provides the local orientation of backward strain-surfaces at the initial time $t=a$ (see Figure 3 for an illustration).

Theorem 1.

- (i) Forward strain-surfaces coincide with backward stretch-surfaces.
- (ii) Backward strain-surfaces coincide with forward stretch-surfaces.

Proof. See Appendix A. □

The following corollary summarizes the implications of Theorem 1, along with known results from Haller (2011) and Farazmand and Haller (2012).

Corollary 1. Let $\mathcal{R}(t)$ and $\mathcal{A}(t)$ be, respectively, repelling and attracting LCSs of the dynamical system (1). Then, the following hold:

- (i) A repelling LCS, $\mathcal{R}(t)$, is a forward strain-surface, i.e., $\mathcal{R}(a)$ is everywhere orthogonal to the eigenvector field ξ_n^f . Furthermore, $\mathcal{R}(t)$ is also a backward stretch-surface, i.e., $\mathcal{R}(b)$ is everywhere orthogonal to the eigenvector field ξ_1^b .

- (ii) An attracting LCS, $\mathcal{A}(t)$, is a forward stretch-surface, i.e., $\mathcal{A}(a)$ is everywhere orthogonal to the eigenvector field ξ_1^f . Furthermore, $\mathcal{A}(t)$ is also a backward strain-surface, i.e., $\mathcal{A}(b)$ is everywhere orthogonal to the eigenvector field ξ_n^b .

Among other things, the above corollary enables the visualization of attracting and repelling LCSs simultaneously at the initial time $t=a$ of a finite time-interval $[a, b]$ over which the underlying dynamical system is known (see Sec. V below for examples). This only requires the computation of the forward-time Cauchy–Green strain tensor C^f , rendering backward-time computations unnecessary. Similarly, the simultaneous visualization of attracting and repelling LCSs at the final time $t=b$ is possible by only one backward-time computation.

We finally comment on the relationship between forward strain-surfaces and classic stable manifolds. If a stable manifold exists for a trajectory through a given initial point p , then the forward strain-surface at p aligns asymptotically with the $t=a$ slice of the stable manifold at p . This is because the stable subspace at p becomes asymptotically the most repelling direction in forward time for all trajectories in the stable manifold. At the same time, trajectories in the unstable manifold through p have no known forward-time asymptotic behavior. Thus, in the general case, forward

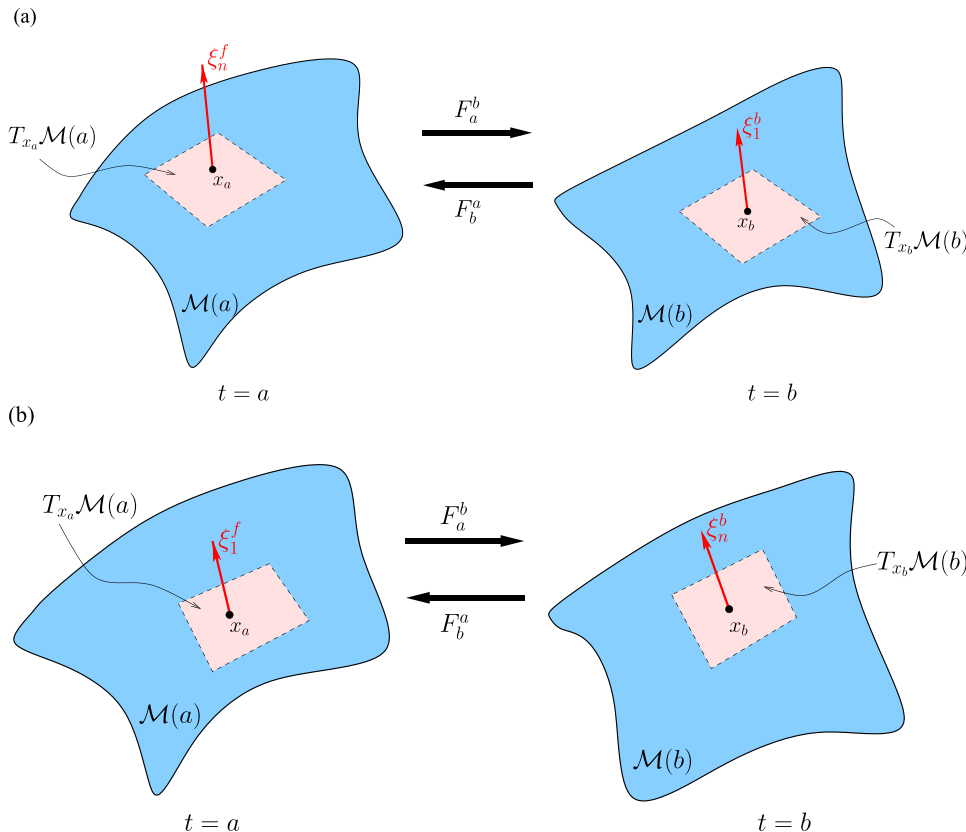


FIG. 3. (a) A forward strain-surface evolves into a backward stretch-surface. (b) A forward stretch-surface evolves into a backward strain-surface.

stretch-surfaces will not align with $t=a$ slices of unstable manifolds. A similar asymmetry holds in backward time: backward strain-surfaces align with unstable manifolds, but backward stretch-surfaces do not align with classic stable manifolds. We will see illustrations of these asymmetries in the examples below.

V. EXAMPLES

Here, we demonstrate the application of Corollary 1 on three examples: the classic Duffing oscillator, a two-dimensional turbulence simulation, and the classic ABC flow. In the two-dimensional case (i.e., $n=2$), we refer to strain- and stretch-surfaces as *strainlines* and *stretchlines*, respectively.

A. Duffing oscillator

Here, we show that even for a two-dimensional autonomous system, stretchlines and strainlines act as *de facto* stable and unstable manifolds over finite time intervals. Indeed, over such intervals, sets of initial conditions will be seen to follow stretchlines in forward time. Only asymptotically do these initial conditions align with the well-known classic unstable manifolds.

Consider the unforced and undamped Duffing oscillator

$$\begin{aligned} \dot{x}_1 &= x_2, \\ \dot{x}_2 &= 4x_1 - x_1^3, \end{aligned} \tag{9}$$

whose Hamiltonian $H(x_1, x_2) = \frac{1}{2}x_1^4 - 4x_1^2 + x_2^2$ is conserved along the trajectories (see Figure 4). The hyperbolic fixed point $(0, 0)$ of the system admits two homoclinic orbits (shown in red), which coincide with the stable and unstable manifolds of the fixed point.

By Definition 1, forward strainlines over a finite time interval are everywhere orthogonal to the eigenvector field ξ_2^f of the forward strain tensor C^f . As a result, strainlines are trajectories of the autonomous ordinary differential equation (ODE)

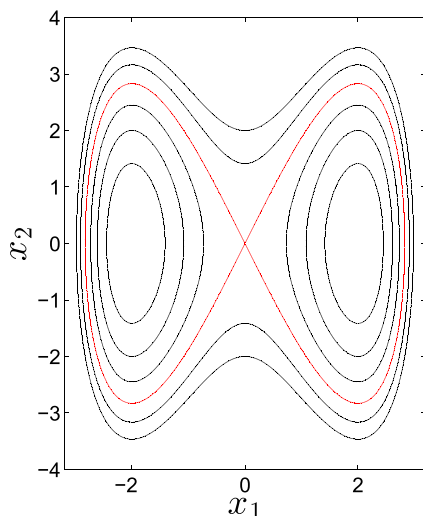


FIG. 4. Trajectories of system (9). The homoclinic orbits are shown in red.

$$r'(s) = \xi_1^f(r(s)), \quad r(0) = r_0, \tag{10}$$

where $r : s \mapsto r(s)$ denotes parametrization by arc-length. Similarly, forward stretchlines are trajectories of the ODE

$$p'(s) = \xi_2^f(p(s)), \quad p(0) = p_0, \tag{11}$$

with $p : s \mapsto p(s)$ denoting an arclength-parametrization. Since we are interested in the *de facto* finite-time stable and unstable manifolds passing through the hyperbolic fixed point $(0, 0)$, we set $r_0 = p_0 = (0, 0)$.

We observe that as the integration time T increases, the unique strainline and the unique stretchline through the origin converge to their asymptotic limits. Figure 5 shows the convergence of these curves around the hyperbolic fixed point $(0, 0)$. For integration times $T \geq 2$, the computed strainlines and stretchlines are virtually indistinguishable from their asymptotic limits. Therefore, in the following, we fix the integration time $T = b - a = 2$ with $a = 0$ and $b = 2$.

Note that while the strainline is indistinguishable from the stable manifold, the stretchline differs from the unstable manifold (see Figure 5(c)). Stretchlines as *de facto* finite-time unstable manifolds define the directions along which passive tracers are observed to stretch. To demonstrate this,

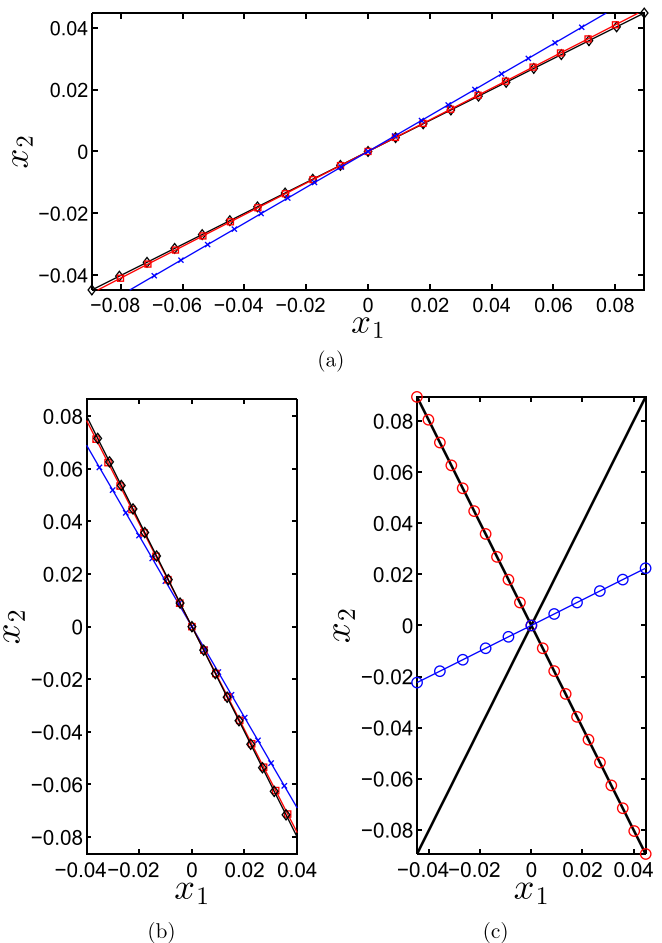


FIG. 5. (a) Forward stretchline through the origin for three integration times $T=0.5$ ($-\times-$), $T=1$ ($-\square-$) and $T=2$ ($-\diamond-$). (b) Forward strainline for the same integration times, as in panel (a). (c) The asymptotic position of the strainline ($-\circ-$) and the stretchline ($-\bullet-$) compared to the classic stable and unstable manifolds (black).

in Figure 6, three disks with radii 10^{-3} , 5×10^{-3} , and 10^{-2} are initially centered at the origin. For short advection times, the tracers elongate in the direction of the stretchline, not the unstable manifold. Unlike the classic unstable manifold, stretchlines evolve in time and only become invariant when viewed in the extended phase space of the (x, t) variables. For longer advection times (not presented here), the stretchline converges to the unstable manifold and becomes virtually indistinguishable from it.

B. Two-dimensional turbulence

We consider a two-dimensional velocity field $u : U \times \mathbb{R}^+ \rightarrow \mathbb{R}^2$, obtained as a numerical solution of the Navier–Stokes equations

$$\begin{aligned} \partial_t u + u \cdot \nabla u &= -\nabla p + \nu \Delta u + f, \\ \nabla \cdot u &= 0, \\ u(x, 0) &= u_0(x). \end{aligned} \quad (12)$$

The domain $U = [0, 2\pi] \times [0, 2\pi]$ is periodic in both spatial directions. The non-dimensional viscosity ν is equal to 10^{-5} .

The forcing f is random in phase and active over the wave numbers $3.5 < k < 4.5$. The initial condition u_0 is the instantaneous velocity field of a decaying turbulent flow. We solve equations (12) by a standard pseudo-spectral method with 512×512 modes. The time integration is carried out by a 4th order Runge–Kutta method with adaptive step-size (MATLAB’s ODE45). Equation (12) is solved over the time interval $I = [0, 50]$.

One can, in principle, compute an attracting LCS at the beginning of a time interval $I = [a, b]$ by advecting the attracting LCS extracted at $t = b$ back to $t = a$. As mentioned in the Introduction, however, this process is numerically unstable since attracting LCSs become unstable in backward time. Their instability is apparent in Figure 7, where an attracting LCS (red) is advected backwards from $t = 50$ to the initial time $t = 0$. The advected curve is noisy and deviates from the true pre-image (blue curve). The true pre-image, the stretchline, is computed as a trajectory of the eigenvector field ξ_2^f of the forward Cauchy–Green strain tensor C^f .

We now extract the set of attracting LCSs that shape observed global tracer patterns in this turbulent flow.

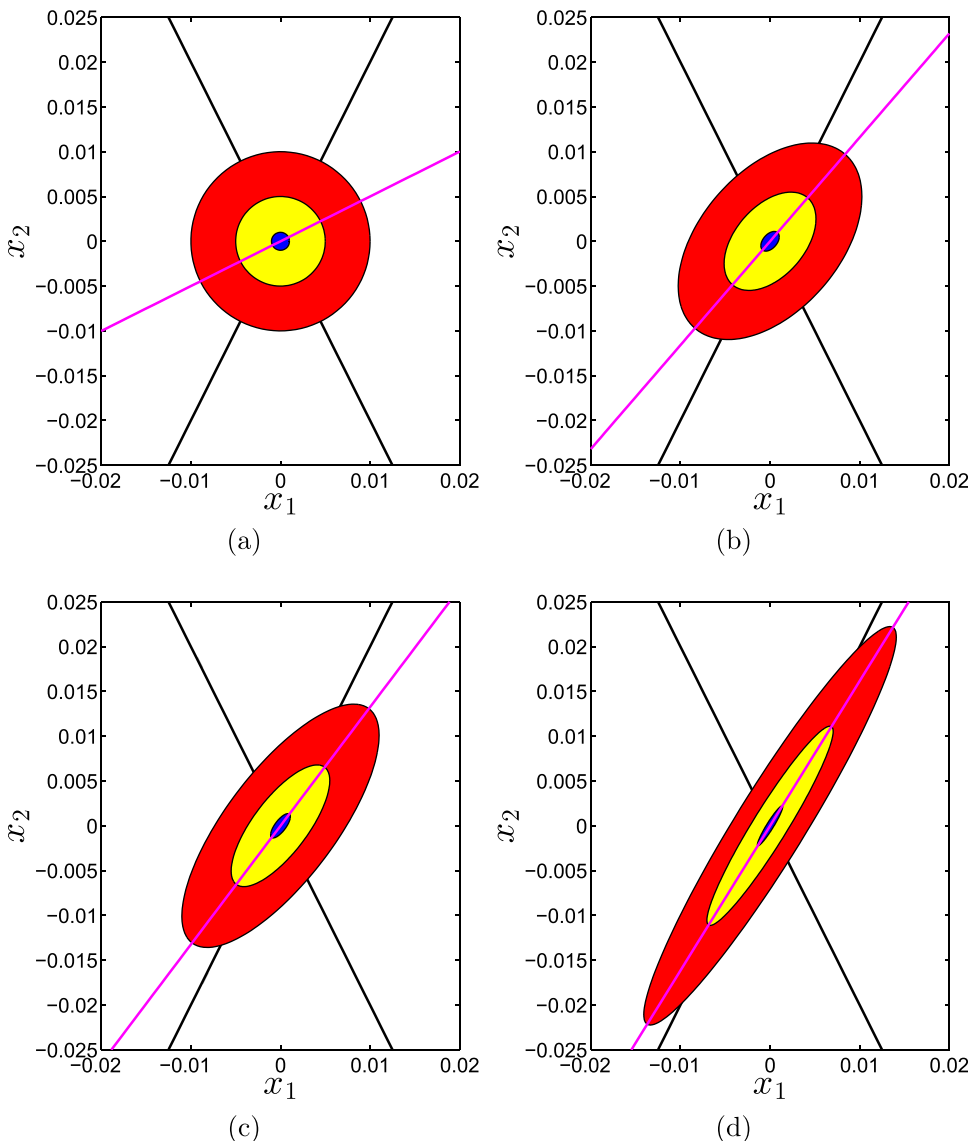


FIG. 6. (a) Classical stable and unstable manifolds (black) are shown together with the stretchline through the origin (magenta). Three blobs of tracers with radii 10^{-3} (blue), 5×10^{-3} (yellow), and 10^{-2} (red) are centered at the origin. The tracers and the manifolds are then advected to time $t = 0.1$ (b), $t = 0.2$ (c), and $t = 0.4$ (d). Over the time interval $[0, 2]$, the stretchline is the de facto unstable manifold for spreading tracers. For larger advection times, this de facto unstable manifold practically coincides the classic unstable manifold of the origin.

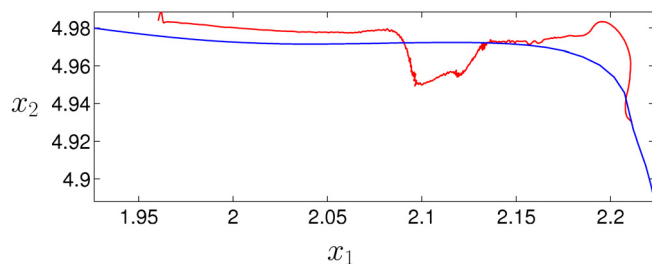


FIG. 7. Stretchline (blue) and the advected image of an attracting LCS (red) at $t=0$. The exponential growth of errors in backward-time advection of the LCS results in a jagged curve that deviates from the true attracting LCS.

Corollary 1 establishes that such LCSs are necessarily forward stretchlines, i.e., trajectories of Eq. (11). It then remains to select the trajectories of this ODE that stretch more under forward advection than any neighboring stretchline (Haller and Beron-Vera, 2012).

The relative stretching of a material line is defined as the ratio of its length at the final time $t=b$ to its initial length at time $t=a$. For a forward-time stretchline γ , one can show (see Appendix B) that the relative stretching is given by

$$q(\gamma) = \frac{1}{\ell(\gamma)} \int_{\gamma} \sqrt{\lambda_2^f} ds, \quad (13)$$

where $\ell(\gamma)$ is the length of γ at time $t=a$. Note that no material line advection is required for computing the relative stretching in Eq. (13).

In order to locate the stretchlines that locally maximize the relative stretching (13), we adopt the numerical procedure outlined in Haller and Beron-Vera (2012) for locating the locally least-stretching strainlines. Specifically, we first compute a dense enough set of stretchlines as the trajectories of ODE (11). We stop the integration once the stretchline reaches a singularity of the tensor field C^f or crosses an elliptic transport barrier.

A *singularity* of C^f is a point where C^f equals the identity tensor, and hence its eigenvectors are not uniquely defined (see Delmarcelle and Hesselink (1994) and Tricoche, Scheuermann, and Hagen (2000) for more details). An *elliptic barrier* is the outermost member of a nested set of closed curves that preserve their initial length (at time $t=a$) under advection up to time $t=b$ (Haller and Beron-Vera, 2012). In an incompressible flow, an elliptic barrier also preserves its enclosed area under advection, and hence the elliptic domain it encloses remains highly coherent. For this reason, elliptic barriers can be considered as generalizations of outermost Kolmogorov–Arnold–Moser (KAM) curves generically observed in temporally periodic two-dimensional flows (Haller and Beron-Vera, 2012).

We locate elliptic barriers using the detection algorithm developed in Haller and Beron-Vera (2012) and Hadjighasem, Farazmand, and Haller (2012). With the location of these barriers and of the singularities of C^f at hand, stretchlines are truncated to compact line segments, rendering the integral in Eq. (13) well-defined. Attracting LCSs at $t=a$ are then located as stretchline segments that have higher relative stretching (13) than any of their C^1 -close neighbors. This process is briefly summarized in the following algorithm:

Algorithm 1.

1. Compute the Cauchy–Green strain tensor C^f over a uniform grid.
2. Locate elliptic barriers by the procedure described in Haller and Beron-Vera (2012); Hadjighasem, Farazmand, and Haller (2012).
3. Compute stretchlines as trajectories of Eq. (11). The initial conditions p_0 are chosen from a uniform grid over the phase space.
4. Stop the stretchline integration once the stretchlines reach either a singular point or an elliptic region bounded by an elliptic barrier.
5. For each stretchline so obtained, compute the relative stretching (13).
6. Locate attracting LCSs as the stretchlines with locally maximal relative stretching.

To illustrate the defining role of stretchlines in the formation of turbulent mixing patterns, we consider three concentric circles of tracers with radii 0.05, 0.1, and 0.2 at the initial time $t=a=0$ (see Figure 8). The circles are centered on a stretchline with locally largest relative stretching (black curve). Then, the stretchlines and tracers are advected to times $t_0=10$, $t_0=15$, and $t_0=25$. In each case, we find that the tracer pattern stretches and aligns with the evolving stretchline, as expected.

We now turn to the global geometry of the attracting LCSs. Figure 9(a) shows stretchlines computed from a uniform grid of 30×30 points. Attracting LCSs at time $t=0$, extracted as stretchlines with the locally largest relative stretching, are highlighted in red. Also shown are the elliptic barriers (green closed curves), as well as a select set of blue tracer disks that will be used to illustrate the role of attracting LCSs. The advected positions of attracting LCSs, elliptic barriers, and tracer disks are shown in Figure 9(b). Note how the attracting LCSs govern the deformation of the tracer disks in the turbulent mixing region. Meanwhile, the elliptic barriers keep their coherence by preserving their arclength and enclosed area.

C. ABC flow

In two dimensions, stretchlines are constructed as trajectories of the eigenvector field ξ_2^f . The resulting curves are, by construction, everywhere orthogonal to the eigenvector field ξ_1^f . In higher dimensions, however, constructing stretch-surfaces that are everywhere orthogonal to the eigenvector ξ_1^f is nontrivial. In fact, for a given eigenvector field, such a surface may only exist locally if a Frobenius condition is satisfied (Lee, 2009). This condition requires the eigenvectors spanning the tangent space of the manifold (here, $\{\xi_k^f\}_{2 \leq k \leq n}$) to be in involution, i.e., their Poisson brackets $[\xi_i^f, \xi_j^f]$ should be in the tangent space of the manifold for any $i, j \in \{2, 3, \dots, n\}$.

Even when the subset of the phase space satisfying this Frobenius condition is known, constructing stretch-surfaces globally as smooth parametrized manifolds normal to a specific vector field is challenging (Palmerius, Cooper, and Ynnerman, 2009; Balzer, 2012). Here, we only illustrate that

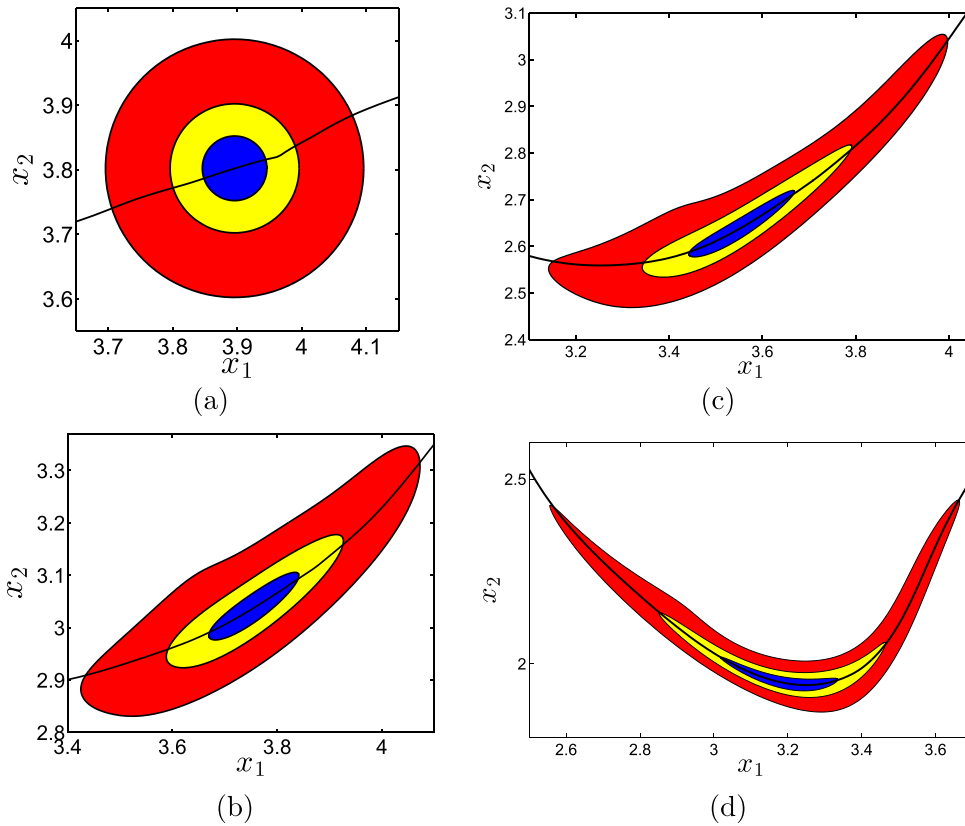


FIG. 8. (a) The concentric tracers with radii 0.05 (blue), 0.1 (yellow), and 0.2 (red). The stretchline (black) passing through the center is computed from the time interval $[0, 50]$ (i.e., $a=0$ and $b=50$). The tracers and the stretchline are then advected forward in time to $t=10$ (b), $t=15$ (c), $t=25$ (d).

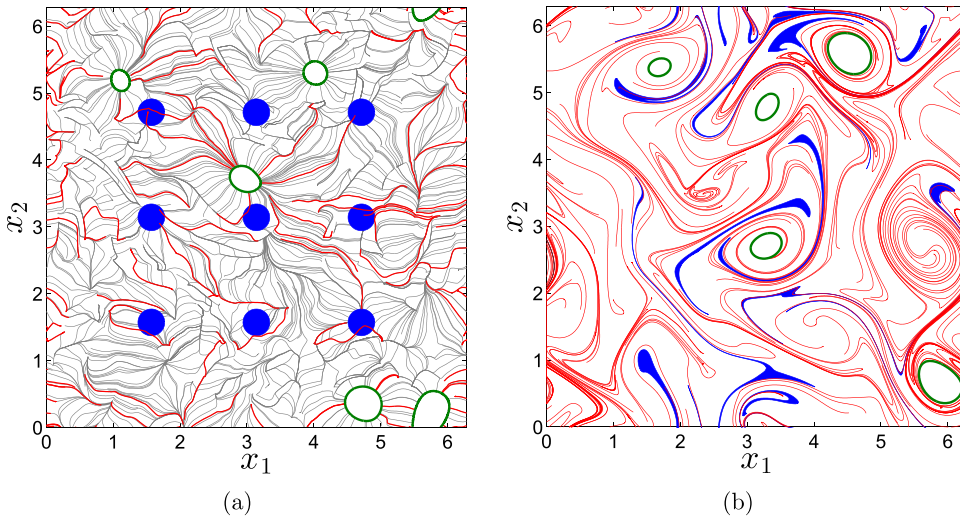


FIG. 9. (a) Forward stretchlines at $t=0$. The attracting LCSs (i.e., locally most-stretching stretchlines) are highlighted in red. The green closed curves show the boundaries of elliptic regions. Tracers (blue circles) are used to visualize the overall mixing patterns. (b) Advected image of the attracting LCSs, tracers, and elliptic barriers at time $t=50$.

locally constructed stretch-surfaces do govern the formation of tracer patterns in three-dimensional flows as well.

We use the classic ABC flow (Arnold and Khesin, 1998)

$$\begin{aligned}\dot{x}_1 &= A \sin(x_3) + C \cos(x_2), \\ \dot{x}_2 &= B \sin(x_1) + A \cos(x_3), \\ \dot{x}_3 &= C \sin(x_2) + B \cos(x_1),\end{aligned}\quad (14)$$

with $A = 1$, $B = \sqrt{2/3}$, and $C = \sqrt{1/3}$. The C^f strain tensor is computed over the time interval $I = [0, 4]$ (i.e., $a=0$ and $b=4$). We release a spherical blob of initial conditions centered at (π, π) with radius 0.1. We approximate the stretch-surface passing through this point by the plane normal to the first eigenvector ξ_1^f of C^f . Figure 10(a) shows this plane together with the sphere of tracers at time $t=0$. The

advected images of the tracer and the plane at time $t=4$ are shown in Figure 10(b), demonstrating that the stretch-surface through the center of the tracer blob acts as a *de facto* unstable manifold in this three-dimensional example as well.

VI. CONCLUSIONS

We have shown that both repelling and attracting LCSs (finite-time stable and unstable manifolds) at a time instance $t=a$ can be extracted from a single forward-time computation over a time interval $I = [a, b]$. This extraction requires the computation of the eigenvectors of the forward Cauchy–Green strain tensor C^f . It has been found previously (Haller, 2011; Haller and Beron-Vera, 2012) that at time $t=a$, the position of repelling LCSs are strain-surfaces, i.e., are everywhere orthogonal to the dominant eigenvector of

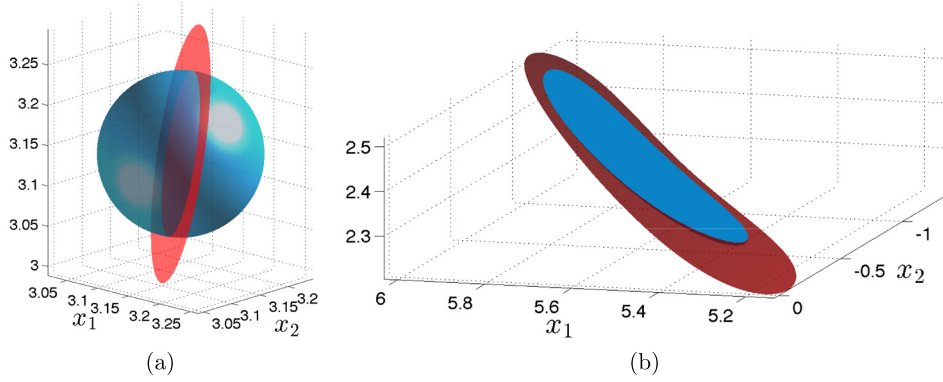


FIG. 10. (a) A spherical tracer surface (blue) at time $t=0$ and the corresponding approximate stretch-surface (red) passing through its origin. (b) The advected positions of these surfaces at the final time $t=4$.

\mathcal{C}^f . Here, we proved that the $t=a$ positions of attracting LCSs are stretch-surfaces, i.e., are everywhere orthogonal to the weakest eigenvector of \mathcal{C}^f .

The attracting LCSs obtained in this fashion are observed as centerpieces around which tracer patterns develop. Even in autonomous dynamical systems, these evolving centerpieces of trajectory evolution differ from classic unstable manifolds, forming *de facto* unstable manifolds over finite times.

In two-dimensional dynamical systems, stretchlines can be directly computed as most-stretching trajectories of the autonomous ODE (11). In higher dimensions, stretch-surfaces satisfy linear systems of partial differential equations (PDEs), as any surface normal to a given vector field does (Palmerius, Cooper, and Ynnerman, 2009). While a self-consistent global solution of these PDEs remains numerically challenging, here we have illustrated the local organizing role of stretch-surfaces through the advection of their tangent spaces in the classic ABC flow. Results on the construction of attracting LCSs from globally computed stretch-surfaces will be reported elsewhere.

ACKNOWLEDGMENTS

G.H. acknowledges partial support by the Canadian NSERC under Grant No. 401839-11.

APPENDIX A: PROOF OF THEOREM 1

In order to prove Theorem 1, we need two lemmas. The first lemma draws a connection between eigenvalues of the forward- and backward-time Cauchy–Green strain tensors. The second lemma establishes a relation between their eigenvectors.

Lemma 1. The largest eigenvalue λ_n^f of the forward-time strain tensor \mathcal{C}^f at a point $x_a \in U$ coincides with the

reciprocal of the smallest eigenvalue λ_1^b of the backward-time strain tensor \mathcal{C}^b at the point $x_b = F_a^b(x_a)$, i.e.,

$$\lambda_n^f(x_a) = \frac{1}{\lambda_1^b(x_b)}. \quad (\text{A1})$$

Similarly, we have

$$\lambda_n^b(x_b) = \frac{1}{\lambda_1^f(x_a)}. \quad (\text{A2})$$

Proof. This follows directly from Eq. (13) in Haller and Sapsis (2011). \square

Lemma 2. For any $x_a \in U$, the following identities hold for any $k \in \{1, 2, \dots, n\}$

$$\begin{aligned} \langle \xi_n^f(x_a), \nabla F_b^a(x_b) \xi_k^b(x_b) \rangle \\ = \lambda_n^f(x_a) \lambda_k^b(x_b) \langle \xi_n^f(x_a), \nabla F_b^a(x_b) \xi_k^b(x_b) \rangle, \end{aligned} \quad (\text{A3})$$

$$\begin{aligned} \langle \xi_n^b(x_b), \nabla F_a^b(x_a) \xi_k^f(x_a) \rangle \\ = \lambda_n^b(x_b) \lambda_k^f(x_a) \langle \xi_n^b(x_b), \nabla F_a^b(x_a) \xi_k^f(x_a) \rangle, \end{aligned} \quad (\text{A4})$$

where $\langle \cdot, \cdot \rangle$ is the Euclidean inner product between two vectors.

Proof. We prove identity (A3). The proof of Eq. (A4) is similar and will be omitted.

First, note that since the flow map is invertible, we have $F_b^a(F_a^b(x_a)) = x_a$ for any $x_a \in U$. Differentiating this identity with respect to x_a , we obtain

$$\nabla F_b^a(x_b) = [\nabla F_a^b(x_a)]^{-1}. \quad (\text{A5})$$

The result then follows from the identity

$$\begin{aligned} \langle \xi_n^f(x_a), \nabla F_b^a(x_b) \xi_k^b(x_b) \rangle &= \langle \xi_n^f(x_a), [\nabla F_b^a(x_b)]^{-1} [\nabla F_b^a(x_b)]^T \nabla F_b^a(x_b) \xi_k^b(x_b) \rangle \\ &= \langle [\nabla F_b^a(x_b)]^{-1} \xi_n^f(x_a), \mathcal{C}^b(x_b) \xi_k^b(x_b) \rangle \\ &= \lambda_k^b(x_b) \langle \nabla F_a^b(x_a) \xi_n^f(x_a), \xi_k^b(x_b) \rangle \\ &= \lambda_k^b(x_b) \langle [\nabla F_a^b(x_a)]^{-1} [\nabla F_a^b(x_a)]^T \nabla F_a^b(x_a) \xi_n^f(x_a), \xi_k^b(x_b) \rangle \\ &= \lambda_k^b(x_b) \langle \mathcal{C}^f(x_a) \xi_n^f(x_a), [\nabla F_a^b(x_a)]^{-1} \xi_k^b(x_b) \rangle \\ &= \lambda_n^f(x_a) \lambda_k^b(x_b) \langle \xi_n^f(x_a), \nabla F_b^a(x_b) \xi_k^b(x_b) \rangle, \end{aligned}$$

where we have used identity (A5) twice. □

Now we turn to the proof of Theorem 1.

Proof of Theorem 1:

- (i) Assume that $\mathcal{M}(t)$ is a backward stretch-surface. Then, by definition, $\mathcal{M}(b)$ is everywhere orthogonal to the eigenvector field ξ_1^b . In order to show that $\mathcal{M}(t)$ is a forward strain-surface, it suffices to show that $\mathcal{M}(a) = F_b^a(\mathcal{M}(b))$ is everywhere normal to the eigenvector field ξ_n^f . Since $T_{x_b}\mathcal{M}(b) = \text{span}\{\xi_k^b(x_b)\}_{2 \leq k \leq n}$ for any $x_b \in \mathcal{M}(b)$, we have

$$T_{x_a}\mathcal{M}(a) = \text{span}\{\nabla F_b^a(x_b)\xi_k^b(x_b)\}_{2 \leq k \leq n},$$

for all $x_a := F_b^a(x_b) \in \mathcal{M}(a)$. Therefore, it suffices to show that $\xi_n^f(x_a) \perp \nabla F_b^a(x_b)\xi_k^b(x_b)$ for any $x_a \in \mathcal{M}(a)$ and $k \in \{2, 3, \dots, n\}$.

From Lemma 2, we have

$$\langle \xi_n^f(x_a), \nabla F_b^a(x_b)\xi_k^b(x_b) \rangle = \lambda_n^f(x_a)\lambda_k^b(x_b)\langle \xi_n^f(x_a), \nabla F_b^a(x_b)\xi_k^b(x_b) \rangle, \quad (\text{A6})$$

for any $x_a \in \mathcal{M}(a)$ and $k \in \{2, 3, \dots, n\}$.

Using identity (A1), we obtain

$$\langle \xi_n^f(x_a), \nabla F_b^a(x_b)\xi_k^b(x_b) \rangle = \frac{\lambda_k^b(x_b)}{\lambda_1^b(x_b)} \langle \xi_n^f(x_a), \nabla F_b^a(x_b)\xi_k^b(x_b) \rangle. \quad (\text{A7})$$

Hence, if

$$\lambda_1^b(x_b) \neq \lambda_k^b(x_b), \quad k \in \{2, 3, \dots, n\}, \quad (\text{A8})$$

then we have

$$\langle \xi_n^f(x_a), \nabla F_b^a(x_b)\xi_k^b(x_b) \rangle = 0, \quad (\text{A9})$$

for any $k \in \{2, 3, \dots, n\}$. But since $\lambda_1^b \leq \lambda_2^b \leq \dots \leq \lambda_n^b$, conditions (A8) hold if and only if $\lambda_1^b(x_b) \neq \lambda_2^b(x_b)$. This condition holds away from repeated eigenvalues of C^b .

In short, if $\xi_1^b(x_b) \perp T_{x_b}\mathcal{M}(b)$ for all $x_b \in \mathcal{M}(b)$ then $\xi_n^f(x_a) \perp T_{x_a}\mathcal{M}(a)$ for any $x_a \in \mathcal{M}(a)$ which implies that $\mathcal{M}(a)$ is a forward strain-surface. This concludes the sufficiency condition of Theorem 1-(i).

As for the necessity of the same condition, let $\mathcal{M}(t)$ be a forward strain-surface, i.e., $T_{x_a}\mathcal{M}(a) = \text{span}\{\xi_k^f(x_a)\}_{1 \leq k \leq n-1}$ for any $x_a \in \mathcal{M}(a)$. Therefore, the tangent space of its advected image $\mathcal{M}(b)$ is given by

$$T_{x_b}\mathcal{M}(b) = \text{span}\{\nabla F_a^b(x_a)\xi_k^f(x_a)\}_{1 \leq k \leq n-1}.$$

To show that $\mathcal{M}(t)$ is a backward stretch-surface, it suffices to show that $\xi_1^b(x_b) \perp \nabla F_a^b(x_a)\xi_k^f(x_a)$ for any $x_b \in \mathcal{M}(b)$ and $k \in \{1, 2, \dots, n-1\}$. Similarly to Eq. (A7), one can show that

$$\langle \xi_1^b(x_b), \nabla F_a^b(x_a)\xi_k^f(x_a) \rangle = \frac{\lambda_k^f(x_a)}{\lambda_n^f(x_a)} \langle \xi_1^b(x_b), \nabla F_a^b(x_a)\xi_k^f(x_a) \rangle, \quad (\text{A10})$$

which implies that $\langle \xi_1^b(x_b), \nabla F_a^b(x_a)\xi_k^f(x_a) \rangle = 0$ for $k \in \{1, 2, \dots, n-1\}$ away from the degenerate points where $\lambda_n^f = \lambda_{n-1}^f$. □

- (ii) The proof is identical to that of part (i).

APPENDIX B: RELATIVE STRETCHING OF STRETCHLINES

Here, we derive formula (13) for the relative stretching of forward stretchlines. Let γ_t be a smooth material line. Denote its time- a and time- b positions by γ_a and γ_b , respectively. Then, the relative stretching of the material line γ_t over the time interval $I = [a, b]$ is defined as

$$q(\gamma_t) := \frac{\ell(\gamma_b)}{\ell(\gamma_a)}, \quad (\text{B1})$$

where ℓ denotes the length of a curve.

Let $r: s \mapsto r(s)$ be the parametrization of γ_a by arc-length, i.e., let $|r'(s)| = 1$ for all $s \in [0, \ell(\gamma_a)]$. Since $\gamma_b = F_a^b(\gamma_a)$, the mapping $F_a^b \circ r: s \mapsto F_a^b(r(s))$ is a parametrization of the curve γ_b . Therefore, its length $\ell(\gamma_b)$ is given by

$$\begin{aligned} \ell(\gamma_b) &= \int_0^{\ell(\gamma_a)} |\nabla F_a^b(r(s))r'(s)| ds \\ &= \int_0^{\ell(\gamma_a)} \sqrt{\langle r'(s), C^f(r(s))r'(s) \rangle} ds. \end{aligned} \quad (\text{B2})$$

Now, if the material line γ_t is a forward stretchline, we have $r'(s) = \xi_2^f(r(s))$ for all $s \in [0, \ell(\gamma_a)]$. Substituting this in Eq. (B2), we obtain

$$\ell(\gamma_b) = \int_0^{\ell(\gamma_a)} \sqrt{\lambda_2^f(r(s))} ds := \int_{\gamma_a} \sqrt{\lambda_2^f} ds.$$

Therefore, by definition (B1), the relative stretching of a forward-time stretchline γ_t is given by

$$q(\gamma_t) = \frac{1}{\ell(\gamma_a)} \int_{\gamma_a} \sqrt{\lambda_2^f} ds.$$

Arnold, V. and Khesin, B., *Topological Methods in Hydrodynamics* (Springer, 1998), Vol. 125.
 Balzer, J., "A Gauss-Newton method for the integration of spatial normal fields in shape space," *J. Math. Imaging Vision* **44**, 65–79 (2012).
 Delmarcelle, T. and Hesselink, L., "The topology of symmetric, second-order tensor fields," in *Proceedings of the conference on Visualization '94* (IEEE Computer Society Press, Los Alamitos, CA, USA, 1994), pp. 140–147.
 Farazmand, M. and Haller, G., "Computing Lagrangian coherent structures from their variational theory," *Chaos* **22**, 013128 (2012).
 Hadjighasem, A., Farazmand, M., and Haller, G., "Detecting invariant manifolds, attractors and generalized KAM tori in aperiodically forced mechanical systems," *Nonlinear Dyn.*, in press, doi 10.1007/s11071-013-0823-x.
 Haller, G., "A variational theory of hyperbolic Lagrangian coherent structures," *Physica D* **240**, 574–598 (2011).
 Haller, G. and Beron-Vera, F. J., "Geodesic theory of transport barriers in two-dimensional flows," *Physica D* **241**, 1680–1702 (2012).
 Haller, G. and Sapsis, T., "Lagrangian coherent structures and the smallest finite-time Lyapunov exponent," *Chaos* **21**, 023115 (2011).
 Haller, G. and Yuan, G., "Lagrangian coherent structures and mixing in two-dimensional turbulence," *Physica D* **147**, 352–370 (2000).

- Lee, J. M., *Manifolds and Differential Geometry*, Graduate Studies in Mathematics (American Mathematical Society, 2009).
- Lekien, F. and Ross, S. D., "The computation of finite-time Lyapunov exponents on unstructured meshes and for non-Euclidean manifolds," *Chaos* **20**, 017505 (2010).
- Lipinski, D. and Mohseni, K., "A ridge tracking algorithm and error estimate for efficient computation of Lagrangian coherent structures," *Chaos* **20**, 017504 (2010).
- Palmerius, K. L., Cooper, M., and Ynnerman, A., "Flow field visualization using vector field perpendicular surface," in *Proceedings of the 2009 Spring Conference on Computer Graphics*, Budmerice, Slovakia, 2009.
- Peacock, T. and Dabiri, J., "Focus issue: Lagrangian coherent structures," *Chaos* **20**, 17501 (2010).
- Tricoche, X., Scheuermann, G., and Hagen, H., "A topology simplification method for 2D vector fields," in *Proceedings of Visualization 2000* (2000), pp. 359–366.